[*ibid.* **91**, 5937 (1969)]. From the experimental sensitivity of Edwards and Raymonda, I concluded that σ (122 nm) $< 3 \times 10^{-19}$ cm^2. Electron impact and photoelectron spectra and the theoretical spectroscopy of CF_4 show no significant absorption bands for $\lambda > 99$ nm [C. Sandorfy, *Atmos. Environ.* **10**, 343 (1976); W. Harshbarger and E. Lassettre, *J. Chem. Phys.* **58**, 1505 (1973); R. Robin, in *Higher Excited States of Polyatomic Molecules* (Academic Press, New York, 1974), vol. 1, pp. 178–191]. To compute CF_4 photodissociation rates, I used solar irradiances from J. Timothy [in *The Solar Output and Its Variation*, O. White, Ed. (Colorado Univ. Press, Boulder, 1977), pp. 237–258].

4. W. Wilson, Jr., and J. O'Donovan, *J. Chem. Phys.* **48**, 2829 (1968). One might also deduce an upper limit for k_1 from the analogous but exothermic insertion into CCl_4 measured by A. Ung and H. Schiff [*Can. J. Chem.* **40**, 486 (1962)]; I obtain $k_1 < 3 \times 10^{-14}$ exp($-7250/T$), that is, smaller than the k_1 in Table 1.
5. Molecular enthalpies for calculating reaction enthalpies were taken from the *Joint Army–Navy–Air Force Thermochemical Tables* (National Bureau of Standards, Gaithersburg, Md., ed. 2, 1971). *The Handbook of Chemistry and Physics* (CRC Press, Cleveland, ed. 58, 1978) erroneously gives $\Delta H^0_{f298} = -162$ kcal mole^{-1} for CF_4 instead of the correct value, -223 kcal mole^{-1}. The *Handbook of Chemistry and Physics* did provide a solubility of CF_4 in water at 25°C of 1.5×10^{-5} (by weight), however.
6. Temperature, N_2 profiles, and O_2 profiles are from *The U.S. Standard Atmosphere* (National Oceanic and Atmospheric Administration, Washington, D.C., 1976). Profiles of O, O(^1D), and H are from S. C. Liu and R. Cicerone's unpublished calculations; OH* and O(^1S) values are from A. Nagy, S. Liu, and D. Baker [*Geophys. Res. Lett.* **3**, 731 (1976)] and T. Donahue, B. Guenther, and R. Thomas [*J. Geophys. Res.* **78**, 6662 (1973)], respectively.
7. Insertion of O into C–F bonds is less likely than for O into CH_4, but the only experimental upper limit on k_4 is 10^{-11} cm^3 sec^{-1} [from R. Atkinson, G. Breuer, J. Pitts, Jr., H. Sandoval, *J. Geophys. Res.* **81**, 5765 (1976)]. I chose k_4, k_5, and $k_6 \leq 10^{-12}$ cm^3 sec^{-1} based on the work of K. Schofield [*J. Photochem* **9**, 55 (1978)] and on discussions with K. Schofield and W. DeMore.
8. For H + $CF_4 \rightarrow$ HF + CF_3, E_a must be larger than the value of 9.5 kcal mole^{-1} found for similar reactions with CH_3Cl and CH_3F by A. Westenberg and N. deHaas [*J. Chem. Phys.* **62**, 3321 (1975)]. Similarly, for H + $CF_3Cl \rightarrow$ HCl + CF_3, J. Bradley, D. Whytock, and T. Zaleski [*J. Chem. Soc. Faraday Trans. 1* **72**, 2284 (1974)] found $E_a = 8.8$ kcal mole^{-1}. Even higher E_a values can be gleaned from Dacey and Hodgins in (*3*) and from V. Kochubei and F. Moin [*Kinet. Catal.* **11**, 712 (1970)].
9. G. Streit and H. Johnston, *J. Chem. Phys.* **64**, 95 (1978).
10. For a C–F bond energy of 129 kcal mole^{-1} (5.61 eV), e + $CF_4 \rightarrow F^-$ + CF_3 is endothermic by 2.27 eV because the electron affinity of F is 3.34 eV [from H. Hotop and W. Lineberger, *J. Phys. Chem. Ref. Data* **4**, 539 (1975)]. By contrast, e + $CFCl_3 \rightarrow Cl^-$ + $CFCl_2$ is exothermic by 0.2 eV.
11. Hydrolysis of perhalocarbons, pyrolysis in high-temperature combustion, dissociation by lightning, and reaction on atmospheric aerosols are discussed in *Halocarbons: Effects on Stratospheric Ozone* (National Academy of Sciences, Washington, D.C., 1976), pp. 179–201; CF_4 is stable at temperatures of at least 1200°C [see (*17*, p. 310)].
12. F. Letkiewicz, *Report EPA-560/8-76-003* (Environmental Protection Agency, Washington, D.C., 1976), pp. 72–73. Although certain African plants can cleave single C–F bonds [R. Hall and R. Cain, *New Phytol.* **71**, 839 (1972)], no known marine natural product contains C–F bonds [J. Faulkner, *Tetrahedron* **33**, 1421 (1977)].
13. The spatial one-dimensional, time-dependent partial differential equation of mass transport with photochemical loss was solved by Crank-Nicolson finite-differencing with $\Delta z = 1$ km and $\Delta t = 30$ days. Eddy-mixing coefficients were from D. Hunten [*Profile A in Chlorofluoromethanes in the Stratosphere* (National Aeronautics and Space Administration, Washington, D.C., 1977), p. 137]. Boundary conditions were as follows: at $z = 0$, a CF_4 input flux was either time-varying as specified in the text, constant for a steady-state calculation, or 0 when an initial CF_4 profile was allowed to decay as a result of sinks; at $z = 90$ km, the upward CF_4 flux is equal to the integrated loss above 90 km from the previous time step. Integrations of 300 years conserved mass to better than 1 percent as did steady-state calculations.
14. R. Stolarski and R. Rundel, *Geophys. Res. Lett.* **2**, 443 (1975); R. Watson, P. Smokler, W. DeMore, *Publication 77-181* (Jet Propulsion Laboratory, Pasadena, Calif., 1977).
15. N. Kameyama, T. Somiya, S. Nagaura, Y. Konishi, paper presented at the 12th International Congress on Pure and Applied Chemistry, New York, 1951; J. Henry and R. Holliday, *J. Met.* **9**, 1384 (1957); T. Somiya and Y. Konishi, *Kogakuin Univ. Res. Rep. 30* (1971), p. 72.
16. C. Slesser and S. Schram, Eds., *Preparation, Properties, and Technology of Fluorine and Organic Fluoro Compounds* (McGraw-Hill, New York, 1951), pp. 31–112; J. Katz and E. Rabinowitch, *The Chemistry of Uranium* (McGraw-Hill, New York, 1951), pp. 126 and 442.
17. H. G. Bryce, in *Fluorine Chemistry*, J. Simons, Ed. (Academic Press, New York, 1964), vol. 5.
18. A. Cottrell, *An Introduction to Metallurgy* (St. Martins, New York, 1967); D. Altman and M. Farber, *Progress Report 9-26* (Jet Propulsion Laboratory, Pasadena, Calif., 1948).
19. A. Goldman, D. Murcray, F. Murcray, G. Cook, J. Van Allen, F. Bonomo, R. Blatherwick, *Geophys. Res. Lett.* **6**, 609 (1979).
20. I thank F. Fehsenfeld, J. Margitan, R. Hampson, G. Ray, F. Rowland, R. Rasmussen, and R. Watson for useful discussions and S. Walters for expert programming. Supported under NSF grant ATM78-26728; the National Center for Atmospheric Research (NSF-supported) provided support for computer time.

8 March 1979; revised 24 May 1979

Deciphering the Scattering Code Contained in the Resonance Echoes from Fluid-Filled Cavities in Solids

Abstract. *From the echoes of elastic waves incident on inclusions in solids, one may extract certain resonance features. These "spectral lines" and their widths form a code identifying the material composition of the inclusion in a way that resembles spectroscopy. This idea finds applications in geophysics, materials science, and any field dealing with materials containing inclusions.*

The amplitudes of backscattered waves returned by inclusions in viscoelastic solids, when plotted as a function of frequency, exhibit so many rapid oscillations and complicated features that until very recently it was not possible to extract the physical information contained in them. The amplitudes of these waves can be analyzed in light of our new resonance theory of scattering from cavities in solids (*1*, *2*) and can be used to identify, for a given shape of the cavity, the material composition of the filler substance. When a (spherical) filler is set into oscillation by elastic (say, compressional) waves incident upon it, a set of modal resonances (fundamental and overtones) gets excited in it; these resonances characterize the filler as if they were its signature. Since incident shear waves excite the same resonances in the filler, we will limit this analysis to incident compressional waves and we shall consider fluid fillers only. From the usual spectral plots of the backscattered wave amplitudes versus nondimensional frequency $x \equiv k_d a$, it is possible to obtain these resonances, which manifest themselves as narrow lines or wider "spikes" ($k_d = \omega/c_d$, where ω is the circular frequency of the incident wave, c_d is the speed of the compressional waves, and a is the cavity radius). These plots display a quantity which, for simplicity, we will call "the echo." The way the resonances of an unknown filler are thus being used for purposes of material discrimination resembles the way chemical elements are identified from their optical spectra. The resonances obtained from the (heretofore physically incomprehensible) echo plot lead directly to a deciphering of the code, indicating the composition of the filler material that is contained in the echo.

Plane p (that is, compressional) elastic waves incident on fluid-filled spherical cavities in solids produce two scattered waves, one compressional and the other shear (that is, s). The scattering amplitudes f^{pp} or f^{ps} of both these scattered waves could be analyzed, but, since all the main points of this report can be shown from either one of these, we choose $f^{pp}(\theta)$. This nonmode-converted, normalized amplitude can be shown (*1*) to be

$$\frac{f^{pp}(\theta)}{a} = \sum_{n=0}^{\infty} \frac{f_n^{pp}(\theta)}{a} = \sum_{n=0}^{\infty} \frac{(2n+1)}{ik_d a} A_n P_n(\cos\theta) \quad (1)$$

where the coefficients A_n are given by ratios of two 3×3 determinants whose elements contain products of the filler-to-matrix density ratio (that is, ρ_f/ρ) with various spherical Bessel and Hankel functions and their derivatives, of arguments $k_d a$ and $k_s a$, and of order n. These elements are determined from the boundary conditions of the problem and are given in (*1*). In the backscattering direction $\theta = \pi$, the Legendre polynominals are simplified by means of the relation $P_n(\cos\pi) = (-1)^n$. Figure 1 shows the plot of the modulus of this summed backscattered amplitude for a cavity filled with ethyl alcohol in an aluminum matrix. This is the "echo" containing the rapid oscillations and complex features mentioned above.

0036-8075/79/1005-0061$00.50/0

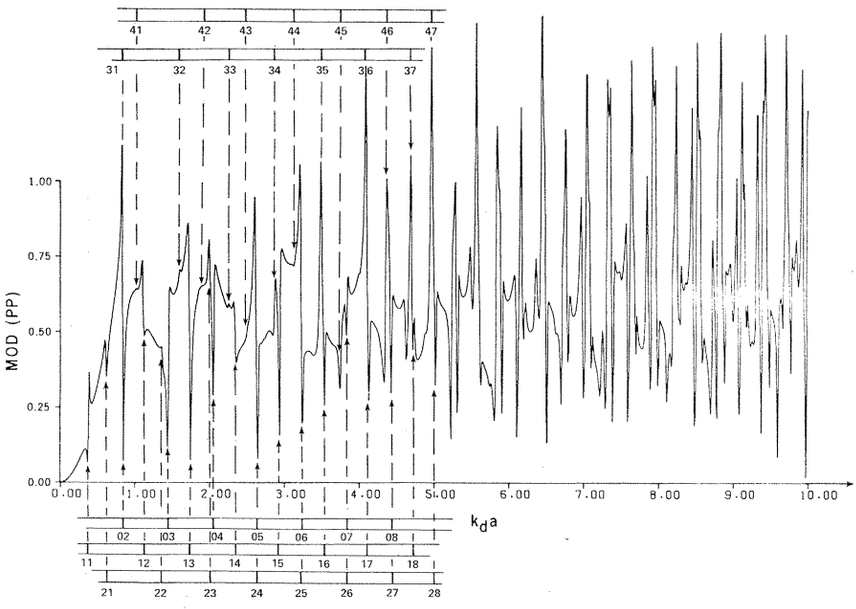

Fig. 1. Modulus of the summed backscattering amplitude f^{pp}/a [denoted MOD(PP)] plotted versus $k_d a \equiv x$, for an alcohol-filled spherical cavity in an aluminum matrix. More than 30 echo oscillations are identified by means of the resonances isolated in Fig. 2, which are labeled by the indices (n, ℓ).

Adding 15 partial waves ($n = 0, 1, \cdots 14$) in the sum of Eq. 1 with $\theta = \pi$ suffices to produce an accurate graph in the range $0 \leq x \equiv k_d a \leq 10$ of Fig. 1.

Considerable simplification is introduced by analyzing each individual partial-wave contribution rather than the summed echo amplitude. The first row of Fig. 2 shows the amplitude moduli $|f_n^{pp}(\pi)/a|$ of the first two ($n = 0, 1$) of the modes, which were added together to obtain the curve in Fig. 1. Each one of these modal contributions can be split into the two portions shown in the second and third rows of Fig. 2, also for alcohol in aluminum. The second row displays the moduli of the smooth "background" contributions (analogous to the "potential scattering" of quantum theory) of an evacuated cavity, which are obtained by repeating the preceding calculations setting $\rho_f = 0$. The third row gives the modulus of the difference of the two aforementioned complex quantities. For each mode n, these resonances are labeled by an index ℓ. The spike labeled $\ell = 1$ in each mode n is the fundamental, and the others ($\ell = 2, 3, \cdots$) are the overtones. Each partial-wave plot can be physically interpreted as the interference between the smooth "potential scattering" background of an empty cavity and the resonances of the filler. There are no approximations involved in the calculation of these figures.

Overlaying each set ($\ell = 1, 2, \cdots$) of resonances for each mode ($n = 0, 1, 2 \cdots$) on top of the summed amplitude of Fig. 1 permits us to identify each extremum in that plot, with the sets of modal resonances contained in each partial-wave contribution. The resonances responsible for each wiggle of Fig. 1 are labeled by indices (n, ℓ), and over 30 wiggles are uniquely identified with resonances in this fashion. Since each substance has its own set of identifying resonances, we could construct a "library of signatures" and compare the echo from each new, unknown filler to the library entries to identify the filler in this fashion. It is not necessary to do this in detail, since there are quicker and more direct methods of identifying the filler from the spacing between high-order overtones and their widths.

In earlier work (*1*), we displayed plots analogous to Fig. 2 but for water (rather than alcohol) in the same aluminum matrix. For the case of water, the set of modal resonances is different from that in Fig. 2; hence, an immediate distinction between the two fillers is quite evident. The location of all the resonance spikes in fact identifies the ratio c_f/c_d of the wave speed of the filler to that of the matrix. The value of c_f can be found from the asymptotic spacing Δ between any two high-order consecutive overtones shown in Fig. 2. For spherical cavities in solids, we have shown (*2*) that Δ (to be read from Fig. 2) becomes uniform for $\ell \gg 1$ and it is $\Delta \approx \pi(c_f/c_d)$. For alcohol in aluminum, that relation gives $\Delta \approx 0.59$ (Fig. 2). Thus, knowing c_d for the matrix and the spacing Δ between consecutive, high-order, modal resonances determines c_f. Conversely, if the filler is known, the size of the cavity is determined. Incidentally, the same formula for the asymptotic spacing is also found to hold for cylindrical cavities.

A dependence of the resonance frequencies on different cavity shapes may be critical, but this may be used for extracting additional information from the echo. The resonance frequencies of a fluid enclosed in a prolate spheroidal cavity are split into two different sets $f_{n\ell}^{(1)}$ and $f_{n\ell}^{(2)}$, corresponding to standing waves along a long or a short axis, respectively. These two sets may be experimentally separated as follows. If a compressional wave incident on the cavity travels along the long (or short) axis, the wave will then excite only the resonances of type $f_{n\ell}^{(1)}$ ($f_{n\ell}^{(2)}$). Traveling in any other direction, it will excite both sets of resonances with weights depending on the direction of incidence. (The effect of an incident shear wave is just the reverse.) This allows a determination of the lengths of the two axes and of the cavity orientation.

For a given cavity shape, one may also determine ρ_f/ρ. This is found from the resonance widths.

The expression for the widths found in our earlier work [equations 34 and 35 of (*1*)] leads to the relation

$$F_n\left(\frac{c_d}{c_f}x\right) = \text{Re } z_1(x) - \frac{\text{Im } z_1(x)}{\Gamma_{n\ell/2}}(x - x_{n\ell}) \qquad (2)$$

where the functions $F_n(x)$ and $z_1(x)$ are also given in (*1*) (equations 26 and 27) and the resonance frequencies $x_{n\ell}$ are the roots of the characteristic equation Re $z_1 = F_n$. Equation 2 can be solved for ρ_f/ρ contained in the expression for F_n. The result can be evaluated at a point one half-width below any resonance peak (that is, at $x = x_{n\ell} - 1/2\,\Gamma_{n\ell} \equiv X_{n\ell}$) and then expanded for $x \gg 1$. In this limit the density ratio admits considerable simplification, and it is eventually found that

$$\frac{\rho_f}{\rho} \xrightarrow[x \gg 1]{} \left[-\frac{1}{x} + \frac{c_d}{c_f}\cot\left(\frac{c_d}{c_f}x - n\frac{\pi}{2}\right)\right]_{x = X_{n\ell}} \approx \left\{-\frac{\pi^2}{\Delta^2}x + \left[\frac{\pi^2}{\Delta^2}\left(\ell + \frac{n}{2} - \frac{1}{2}\right)\Delta - \frac{1}{\left(\ell + \frac{n}{2} - \frac{1}{2}\right)\Delta}\right]\right\}_{x = X_{n\ell}} \qquad (3)$$

where the last expression holds for any integer mode order n; and for ($\Gamma n\ell/2) < \Delta$, the latter conditions means that the resonance half-width must be smaller than the asymptotic spacing, so that con-

secutive resonances do not overlap. In this limit, the zeroes of the first expression in Eq. 3 are the zeroes of the cotangent which occur at integer or half-integer multiples of Δ (that is, $x_{n\ell} \overrightarrow{x \gg 1} \ell + n/2 - 1/2)\Delta$, where ℓ is the integer index labeling the pertinent high-order overtone of any mode n). The indicated evaluation in Eq. 3 yields

$$\frac{\rho_f}{\rho} \overrightarrow{x \gg 1} - \frac{1}{\left(\ell + \frac{n}{2} - \frac{1}{2}\right)\Delta} + \frac{\pi^2}{\Delta^2} \frac{\Gamma n\ell}{2} \ldots (n, \ell, = \text{integers}) \quad (4)$$

which in the high-frequency limit gives ρ_f/ρ in terms of Δ and the width $\Gamma_{n\ell}$ of any (high-index) overtone ℓ of any mode n. These are all either known or previously determined quantities. The graphs of the function inside the curly brackets of Eq. 3 plotted versus x are steep in the vicinity of the resonances $x_{n\ell} \approx (\ell + n/2 - 1/2)\Delta$, at which points they go through zeroes. Therefore, the evaluation points one half-width below these resonances must be accurately determined in order to obtain good estimates of the density ratio as given in Eq. 4. For ethyl alcohol ($\rho_f = 0.79$ g/cm^3, $c_f = 1.213 \times 10^5$ cm/sec) in aluminum ($\rho = 2.70$ g/cm^3, $c_d = 6.420 \times 10^5$ cm/sec), we find $\Delta \approx 0.593$ and $\pi^2/\Delta^2 = 28.01$. For the first ($n = 1$) mode, the width of its tenth overtone ($\ell = 10$), which occurs at $x_{n\ell} \approx \ell\Delta = 5.93$, is $\Gamma_{n\ell} \approx 0.06$. This width is $3^{1/2}$ too large (*2*) since it is read from a plot of $|f_n^{pp}|$ rather than from a plot of $|f_n^{pp}|^2$, which is where the widths are commonly defined. Substituting these values into Eq. 4 yields $\rho_f/\rho = 0.296$, which contains about a 1 percent error when compared to the actual ratio 0.79/2.70. Thus, with ρ for the matrix known, the simple relation in Eq. 4 gives the filler density ρ_f. The filler fluid is completely identified once its sound speed and density are determined by this asymptotic procedure.

One can use the method we describe here to determine the material properties of a fluid contained in a (spherical) cavity inside a solid by analyzing the resonances in the amplitude of elastic waves scattered by the cavity. The resonance positions and their widths are used to determine the sound speed and the density of the filler. The sound speed is found from the spacing between two consecutive overtones of any mode, which asymptotically becomes uniform for the higher-index overtones. The density is obtained from the width of any high-order resonance by means of Eq. 4. Therefore, for a given cavity shape, all the information about the material composition of the filler can be extracted, from the (high-frequency) asymptotic region $x \gg 1$ (or $\ell \gg 1$).

This analysis is based on our (*1*, *2*) resonance theory of elastic wave scattering from fluid-filled cavities in solids. Subtracting a suitable nonresonant background from the contribution of each partial wave to the echo from a fluid-filled cavity in a solid, we can determine the resonances of each normal mode and give a physical meaning to the individual partial waves as interferences between backgrounds and resonances. The family

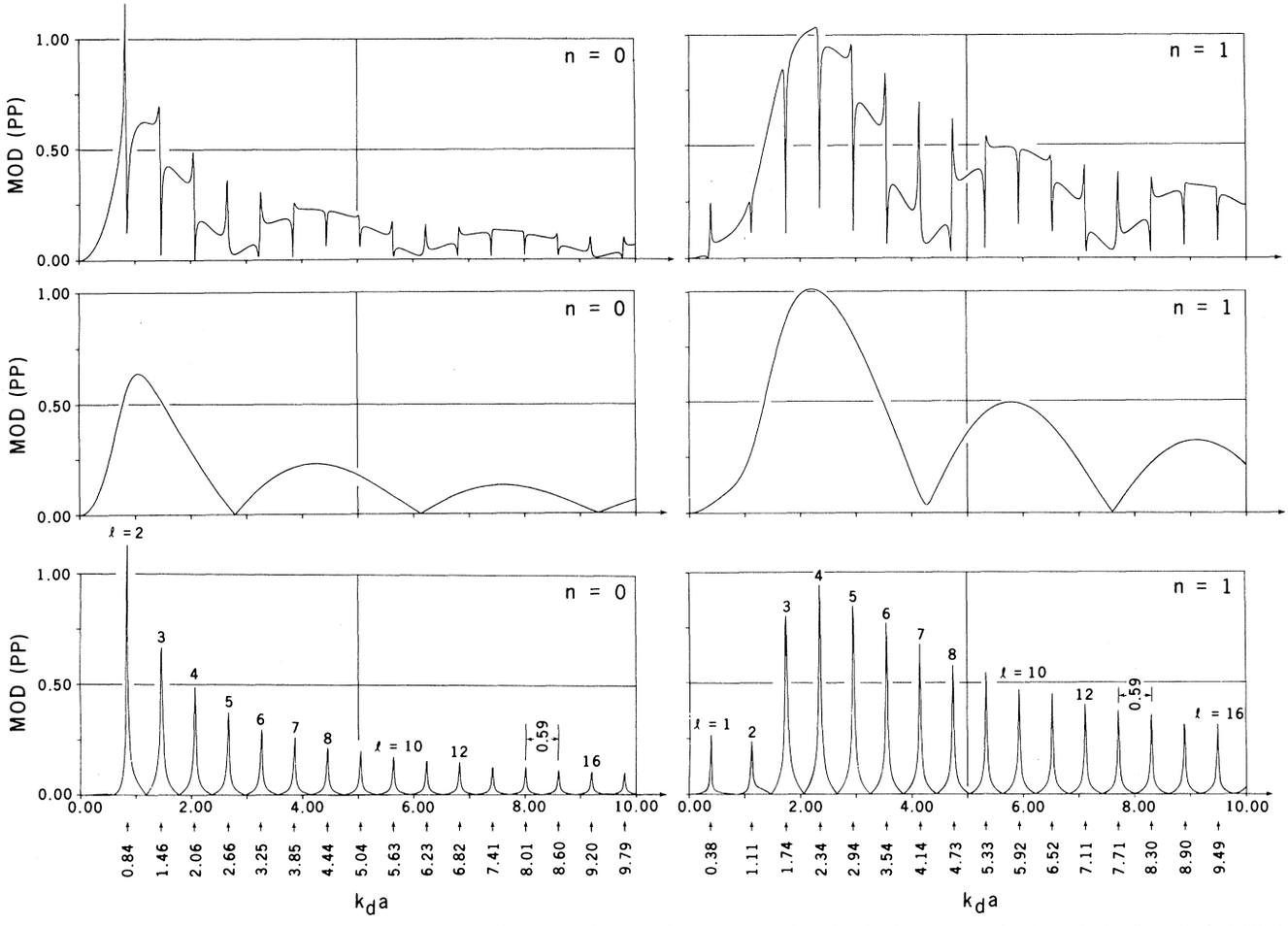

Fig. 2. Resonances (third row, labeled by the index ℓ) of the modulus $|f_n^{pp}/a|$ versus $x \equiv k_d a$, for the first two modes ($n = 0, 1$) of an alcohol-filled spherical cavity in aluminum. The resonances are the result of subtracting the smooth "backgrounds" in the second row from the composite modal contributions in the first row.

of spectral resonances thus found is used to specifically determine which resonance spike in which particular normal mode causes each rapid oscillation in the cavity's summed amplitude $|f^{pp}|$. Making bistatic (that is, away from the monostatic $\theta = \pi$ direction) determinations of $|f^{pp}(\theta)/a|$ from Eq. 1 at angles θ_{nm} chosen to be the zeroes of P_n (cos θ) for a given n, we can eliminate the contribution from that n^{th} mode to the summed amplitude in Eq. 1. In this way bistatic measurements or calculations can be used to suppress and further disentangle the selected individual contribution of any given mode n from the sum of all the others. The use of this theory to decipher the scattering code about material composition contained in the cavity's echo has applications to a variety of problems in geophysics, nondestructive material testing, oil prospecting, and also to scattering from bubbles in liquids or from certain fluidlike substances (namely, tumors) in animal tissue.

GUILLERMO C. GAUNAURD
Naval Surface Weapons Center, White Oak Laboratory, Silver Spring, Maryland 20910
HERBERT M. ÜBERALL
Naval Surface Weapons Center and *Physics Department, Catholic University, Washington, D.C. 20064*

References and Notes

1. G. Gaunaurd and H. Überall, *J. Acoust. Soc. Am.* **63**, 1699 (1978).
2. ———, *J. Appl. Phys.* **50**, 4642 (1979).
3. We thank J. Barlow from our center's computational group for his assistance in preparing the figures. We thank our center's Independent Research Board and Code 421 of the Office of Naval Research for financial support and encouragement.

27 February 1979

Metabolism of Americium-241 in Man: An Unusual Case of Internal Contamination of a Child and His Father

Abstract. *The metabolism of americium-241 has been studied during an 8-year period in an adult male and his son who, at the ages of 50 and 4 years, respectively, were accidentally and unknowingly contaminated within their home by means of inhalation. Chelation therapy with calcium trisodium pentetate was more effective in enhancing the removal of americium-241 from the child than from the father.*

During the past 8 years, sequential measurements have been made of the internal americium-241 burdens of an adult male and his son. Both are believed to have received significant exposures in their home beginning in 1964, when the adult was about 50 and his son about 4 years old. Their contamination was discovered at our laboratory in 1970, when the man and child were approximately 57 and 10 years old, respectively (*1*). Since then, the content and the distribution of ^{241}Am in both subjects have been determined one or more times per year in a whole-body counting facility with a low background, using two or three thin NaI(Tl)-CsI(Tl) Laurer detectors (*2*). These detection systems are specifically designed to measure low-energy, photon-emitting nuclides while minimizing contributions from Compton scattering background radiations with pulse-shaping coincidence electronics.

Americium-241 (half-life, 433 years) is an alpha particle–emitting actinide that also emits a 59.6-keV gamma ray in 36 percent of all decays, permitting its determination in vivo by external counting. Since ^{241}Am is a trivalent actinide which, on entering the body, is deposited primarily in the liver and on skeletal surfaces (*3*), detectors were positioned in configurations so that measurements could be made of ^{241}Am in the whole body, the thorax (lung), the liver, and the head (skull). Results of these measurements, as determined from 1970 through 1977, are listed in Table 1. In 1970, values for the whole body content for the man and his son were 180 and 72.8 percent, respectively, of the maximum permissible occupational body burden of 50 nCi for an adult male (*4*).

Most of the exposure presumably occurred by inhalation, since (i) approximately 44 nCi of ^{241}Am was measured on the basement air-conditioning filter in 1970; (ii) the gastrointestinal absorption factor for ^{241}Am is reported to be less than 10^{-4} (*4*); (iii) the original source activity was reported to be approximately 50 mCi, most of which is still on the recovered source planchet (*5*); and (iv) early clearance of ^{241}Am from the lung of the father was observed. Furthermore, it could be ascertained that the major part of the total exposure occurred sometime in 1964 by determining the ^{241}Am content of the youngster's deciduous teeth and by estimating formation and shedding times of the various teeth types (*6*).

The estimated lung burdens for ^{241}Am in the adult and his son in 1970 were 14.9 and 7.8 nCi, respectively; these values are approximately 93 and 49 percent of the occupational lung burden limit of ~ 16 nCi for an adult. Estimates for lung deposits were made from measurements with two detectors positioned over the anterior thorax. The contribution to this count rate from activity associated with the rib cage structure was determined from measurements of ^{241}Am in skull bones and from the assumption of a similar concentration throughout the thoracic bone structure (*7*).

Liver burden estimates were made in

Table 1. Estimation and sequential measurements of ^{241}Am distribution in an adult male and an adolescent male.

Months since April 1970*	Adult ^{241}Am burden† (nCi)				Adolescent ^{241}Am burden† (nCi)			
	Lung	Liver	Skeleton‡	Total body	Lung	Liver	Skeleton	Total body
0	14.9	3.0	(70.1) 72.1	90.0	7.8	10.0	17.9	36.4
12	15.5	2.6	(75.9) 38.8	56.9	4.6	5.2	9.9	19.7
17	19.4	3.1	(74.7) 33.6	56.1	4.0	5.2	13.9	23.1
29	12.7	4.9	(70.1) 54.6	72.2	3.8	6.5	13.0	23.3
37	16.4	2.9	54.0	73.3	3.1	4.1	19.1	26.3
38	16.3	5.2	46.5	68.0	2.8	6.4	12.1	21.3
42	11.7	1.6	48.0	61.3	2.1	4.2	11.7	18.0
52	12.3	1.3	(40.2) 42.4	56.0	0.3	3.8	14.7	18.8
57	10.4	0.7	(34.5) 50.2	61.3	N.D.§	2.6	15.9	18.5
58	11.5	1.5	(40.2) 41.3	54.3	0.3	1.8	10.1	12.2
75	9.3	0.4	(48.4) 49.9	59.6	N.D.	2.3	10.7	13.0
93	9.3	1.5	(45.3) 44.3	55.6	0.1	1.7	10.5	12.3

*Decorporation therapy was administered during the periods between months 0 and 12, 37 and 38, and 57 and 58. †No error terms have been assigned to these values, since it was determined that unknown positioning consistency, body size variability, detector refabrication, and changing biological distribution of ^{241}Am will all account for errors that may be larger than counting statistics alone. ‡Values in parentheses are determined by extrapolation of skull measurement. Other values are determined as skeleton = total body + lung + liver; values so obtained for 12 and 17 months may be in error because of detector refabrication and calibration change. §Not determined.

0036-8075/79/1005-0064$00.50/0